remote sensing

MDPI

Technical Note

Impacts of Aerosol Chemical Composition on Cloud Condensation Nuclei (CCN) Activity during Wintertime in Beijing, China

Quan Liu [1], Xiaojing Shen [1], Lei Li [1], Junying Sun [1,*], Zirui Liu [2], Weibin Zhu [2], Junting Zhong [1], Yangmei Zhang [1], Xinyao Hu [1,3], Shuo Liu [1,3], Huizheng Che [1] and Xiaoye Zhang [1]

[1] State Key Laboratory of Severe Weather & Key Laboratory of Atmospheric Chemistry of CMA, Chinese Academy of Meteorological Sciences, Beijing 100081, China; liuq@cma.gov.cn (Q.L.); shenxj@cma.gov.cn (X.S.); lilei@cma.gov.cn (L.L.); zhongjt@cma.gov.cn (J.Z.); ymzhang@cma.gov.cn (Y.Z.); huxinyao21@mails.ucas.ac.cn (X.H.); liushuo212@mails.ucas.ac.cn (S.L.); chehz@cma.gov.cn (H.C.); xiaoye@cma.gov.cn (X.Z.)

[2] State Key Laboratory of Atmospheric Boundary Layer Physics and Atmospheric Chemistry, Institute of Atmospheric Physics, Chinese Academy of Sciences, Beijing 100029, China; liuzirui@mail.iap.ac.cn (Z.L.); zhuweibin21@mails.ucas.ac.cn (W.Z.)

[3] College of Earth and Planetary Sciences, University of Chinese Academy of Sciences, Beijing 100049, China

* Correspondence: jysun@cma.gov.cn

Abstract: The cloud condensation nuclei (CCN) activity and aerosol chemical composition were concurrently measured via a scanning mobility CCN analyzer (SMCA) and an Aerodyne Time-of-Flight Aerosol Chemical Speciation Monitor (ACSM), respectively, during wintertime 2022 in Beijing, China. During the observation period, the mean CCN number concentrations ranged from 1345 ± 1270 cm^{-3} at SS = 0.1% to 3267 ± 2325 cm^{-3} at SS = 0.3%. The mean critical activation diameters (D_{50}) at SS = 0.1%, 0.2%, and 0.3% were 172 ± 13 nm, 102 ± 8 nm, and 84 ± 7 nm, corresponding to the average hygroscopicity parameters (κ_{CCN}) of 0.34, 0.33, and 0.26, respectively. The diurnal variations in D_{50} suggested that the local primary emissions significantly enhanced D_{50} at SS = 0.2% and 0.3%, but had less influence on D_{50} at SS = 0.1% due to the limited size (<150 nm) of particles emitted from primary sources. As $PM_{2.5}$ concentration increases, the dominant driver of CCN activity transitions from sulfate to nitrate. At a specific SS, D_{50} decreased with increases in the degree of internal mixing, implying that the elevated internal mixing degree during atmospheric aging was beneficial to CCN activation. In this study, the commonly used $f44$ (or O:C) was weakly correlated with κ_{org} and failed to describe the variations in κ_{org}. Instead, the variations in κ_{org} can be well parameterized with the Org/BC ratio. The correlation between κ derived from bulk chemical compositions and CCN measurements was substantially improved when this κ_{org} scheme was adopted, emphasizing the importance of considering κ_{org} variations on deriving κ_{chem} from aerosol chemical composition.

Keywords: size-resolved CCN activity; aerosol chemical composition; mixing state; organic hygroscopicity

Citation: Liu, Q.; Shen, X.; Li, L.; Sun, J.; Liu, Z.; Zhu, W.; Zhong, J.; Zhang, Y.; Hu, X.; Liu, S.; et al. Impacts of Aerosol Chemical Composition on Cloud Condensation Nuclei (CCN) Activity during Wintertime in Beijing, China. *Remote Sens.* **2023**, *15*, 4119. https://doi.org/10.3390/rs15174119

Academic Editors: Jing Li, Yannian Zhu, Zeen Zhu and Jinming Ge

Received: 27 July 2023
Revised: 15 August 2023
Accepted: 16 August 2023
Published: 22 August 2023

1. Introduction

Aerosol particles can serve as cloud condensation nuclei (CCN) under supersaturation (SS) conditions [1,2], participating in cloud processes and altering the microphysical and optical properties of clouds, which indirectly affect the global climate [3,4]. The Sixth Assessment Report from IPCC (2021) highlighted that aerosol indirect effects remain the most considerable uncertainty in evaluating the anthropogenic contribution on current and future climate change [5]. Remote sensing has been widely used to study aerosol–cloud–climate interactions and provide extensive datasets. However, it is difficult to identify the proportion of CCN from retrieved total aerosol concentration (CCN activation

ratio), which would introduce uncertainties in estimating aerosol-related effects on cloud microphysics based on remote sensing. Furthermore, accurate retrievals of cloud droplet number concentrations (N_d) using remote sensing measurements is challenging. Based on the ground-level measurements of aerosol activation properties and parcel theory, the N_d for non-precipitating Planetary Boundary Layer clouds can be derived. Then, the parameters of the retrieval can be optimized through the closure analysis on N_d obtained from remote sensing data and in situ measurement at ground level [6].

The ability of aerosol particles to participate in cloud processes, known as CCN activity, is one of critical parameters in studying the indirect radiation effects and environmental impacts of aerosols. At a given SS condition, the CCN activity is mainly determined by their size distribution, chemical composition, and mixing state [7–9]. Previous studies suggested that the size distribution of aerosols is a more critical factor than their chemical composition in governing CCN activity [2,10]. However, the impact of chemical composition on CCN activity significantly increases in situations with low supersaturation [11,12]. The classical Köhler theory [1], combining the Raoult's law effect with the Kelvin effect, illustrates that the aerosol particle activation depends on particle size, chemical composition, and SS. Petters and Kreidenweis [13] developed a single hygroscopicity parameter κ in parameterizing the Raoult term, which enabled the quantification of CCN activity without requiring information of the dissolved compounds. However, ambient aerosols are complex mixtures, and their sizes and compositions vary at different stages of atmospheric aging process [14–16], which include numerous primary and secondary organic components as well. These impose various effects on particle activation behavior and reduce the applicability of the Köhler theory in describing the actual atmospheric aerosols, especially for organic aerosols (OA). Earlier studies specifically focused on parametrizing the empirical correlations between the OA oxidation level and organic hygroscopicity parameter (κ_{org}) [17–21], suggesting a linear correlation between κ_{org} and the oxygen-to-carbon atomic ratio (O:C). However, the systematic variability in parametrizations between κ_{org} and the O:C ratio determined from the different studies remains large [22]. Kuang et al. (2021) recently pointed out that secondary OA (SOA) from different precursors and formation processes may result in SOA with different chemical composition, functional properties, and microphysical structure, consequently exerting distinct influences on κ_{org} and rendering single oxidation level parameters (such as O:C) unable to capture those differences [23].

To obtain regional parameters for aerosol particle activation, numerous field campaigns have been conducted globally. Alongside the considerable spatial heterogeneity, temporal variability in aerosol activation characteristics is also essential for accurate CCN prediction [7]. The CCN activity can be characterized by two important parameters: activation critical diameter (D_{50}) and activation ratio (AR). These two parameters can be directly measured through combining cloud condensation nuclei counter (CCNc) and scanning mobility particle sizer (SMPS) [24,25], and can also be determined by aerosol chemical composition and particle number size distribution (PNSD) measurements using the Köhler equation and internal mixture hypothesis [20,26–28]. The CCN activity closure analysis, based on the above two methods, is a key means of investigating the impacts of aerosol properties on activation processes. Although CCN measurements were conducted under different environments in the North China Plain, only a few studies established a linkage between CCN activity and chemical composition with a high time resolution [27,29–31]. Additionally, due to the Clean Air Action of the Chinese government initiated in 2013, stringent emission controls have been imposed to decrease fine particulate matter pollution ($PM_{2.5}$, particles smaller than 2.5 μm in diameter) [32]. In the Beijing region, notable reductions in $PM_{2.5}$ concentration over the past decade have been accompanied by significant changes in its chemical composition [33–35]. Instead of organics and sulfate, organics and nitrate are now the dominant components of Beijing winter haze pollution. Therefore, more investigations are needed to further understand the impacts of these variations on CCN activity in urban Beijing.

In this study, the CCN activity and aerosol chemical composition were simultaneously measured in Beijing wintertime, using a scanning mobility CCN analyzer (SMCA) and an Aerodyne aerosol chemical species monitor (ACSM). An overview of the observation data is presented in Section Overview the Observation Data. The impacts of aerosol chemical composition and mixing state on CCN activity are discussed in Section 4.1. Finally, in Section 4.2, through closure analysis of the aerosol hygroscopicity derived from CCN activity and chemical composition, we estimate κ_{org} and parameterize it with the concentration ratio of organics to BC (Org/BC).

2. Materials and Methods

2.1. Measurement Site

Measurements of size-resolved CCN activity, aerosol size distribution and composition (organics, nitrate, sulfate, ammonium, chloride, and black carbon) were conducted on the rooftop of the Chinese Academy of Meteorological Sciences (CAMS) building during the period of 15 January–3 March 2022. All aerosol measurements were performed downstream of a PM_{10} impactor. The ambient air passes through the impactor and then enters the automatic regenerating adsorption aerosol dryer (TROPOS, Leipzig, Germany), which can dry the sample air to a low RH (RH < 30%) to ensure comparability of measurements [36]. The measurement site (116°19′E, 39°57′N, approximately 53 m above the ground) is located in a traffic-intensive area of the west 3rd ring road in Beijing, China, which represents the urban environment influenced by intense anthropogenic emissions [37,38].

2.2. Instrumentation

2.2.1. Size-Resolved CCN Activity and PNSD Measurements

Size-resolved CCN spectra and activation ratios were measured using the SMCA initially proposed by Moore et al. (2010) [39]. In this work, the SMCA consisted of a CCNc-100 (DMT Inc., Blouder, CO, USA), a differential mobility analyzer (DMA, model 3081, TSI Inc., Shoreview, MN, USA), and a condensation particle counter (CPC, model 3772, TSI Inc.). In the SMCA system, the combined DMA and CPC were used as a SMPS during the measurements. The dry particles after the diffusion dryer were neutralized by the X-ray neutralizer and were subsequently classified by the DMA in a scanning mode. Then, the particles were split into two streams: one to the CPC for measurement of total particle number concentration (N_{CN}) and another to the CCNc-100 for measurements of the CCN number concentration (N_{CCN}). The flow rates of the CPC and CCNc-100 were 1.0 L min^{-1} and 0.5 L min^{-1}, respectively. With the total sample flow of 1.5 L min^{-1} and sheath flow of 7.5 L min^{-1}, the SMCA was protocolled to measure particles at a mobility diameter range of 8–360 nm. The DMA was operated in scanning mode with a time resolution of 180 s, including a scan time of 165 s and a retrace time of 15 s. The supersaturation in the CCNc-100 was set to be 0.1%, 0.2%, and 0.3%, respectively, with a time interval of 9 min (corresponding to three diameter scans of the DMA) for each SS during the experiment. Only the second scan for each SS is used as the CCNc needs time for SS stabilization. Therefore, a complete SS cycle lasted ~0.5 h. The CCNc-100 was regularly calibrated with ammonium sulfate particles at the four SSs (0.1%, 0.2%, 0.4%, and 0.7%).

2.2.2. Aerosol Chemical Composition Measurement

Non-refractory particulate matter (NR-PM) including sulfate, nitrate, ammonium, and organics with dry aerodynamic diameters below 2.5 μm was measured by an ACSM equipped with a $PM_{2.5}$ aerodynamic lens at 10 min time resolution. The ACSM data were analyzed using standard data analysis software (Tofware v2.5.13). The collection efficiency (CE), which accounts for particle loss due to bouncing off the standard vaporizer, was derived from composition-dependent calculation following the algorithms proposed by Middlebrook et al. (2012) [40]. The calibrations of ionization efficiency (IE) and relative ionization efficiencies (RIEs) followed the standard procedures described in previous studies by using 300–350 nm pure ammonium nitrate and ammonium sulfate particles [41,42]. The

RIE values used for organics, sulfate, nitrate, ammonium, and chloride were 1.4, 1.2, 1.1, 3.4, and 1.3, respectively.

Equivalent black carbon (eBC) mass was measured with an aethalometer (AE33, MAGEE Scientific, Berkeley, CA, USA) at 1 min. The instruments used dual-dots configuration to auto-correct for the loading effect. The measured absorption was converted to BC mass using an apparent mass absorption cross section (MAC) of 7.7 m^2 g^{-1} at a wavelength of 880 nm [43]. The λ = 880 nm is chosen to avoid the potential interference of brown carbon at shorter wavelength. The multi-scattering enhancement factor (C value) of 2.88 at 880nm wavelength was used to exclude the multiple light scattering effects.

In addition, $PM_{2.5}$ mass concentration data from air quality monitoring station (Wanliu) operated by the Beijing Municipal Ecology and Environment Bureau were used, which is located in the northwest and northeast direction of the CAMS observation site, with a distance of approximately 3 km. The concurrent meteorological parameters (including wind speed, wind direction, relative humidity, and air temperature) are from the national surface meteorological observation stations of the China Meteorological Administration.

2.3. Data Processing

2.3.1. CCN Activation

The N_{CN} and N_{CCN} data were used to calculate the size-resolved CCN activation ratio (AR), which defined as the ratio of N_{CCN} to N_{CN} at each particle size (N_{CCN}/N_{CN} vs. D_p). The influence of multiple-charge particles and DMA transfer function on AR were corrected basing on a modified algorithm developed by Hagen and Alofs (1983) [44] and Deng et al. (2011, 2013) [25,45]. Figure S1 gives a typical example of N_{CCN}/N_{CN} vs. D_p during the experiment, and the AR curve can be obtained by fitting the N_{CCN}/N_{CN} ratio with the sigmoidal function:

$$\mathrm{AR} = a + b/(1 + \exp\left(\frac{D_{50} - D_p}{\sigma_s}\right)) \quad (1)$$

where a is the offset from 0 in the y direction and b is the height of the upper plateau of the sigmoid function, D_{50} is the critical diameter, and σ_s is a measure for the width of the sigmoid function. D_{50} is also called the critical diameter or the activation diameter, that is, the diameter at which 50% of the particles are activated at a specific SS. The variation in D_{50} at a given SS can be attributed to the variation in the number fraction of hygroscopic particles or its hygroscopicity, which can be indicated the CCN activity of a particle population. Then, the hygroscopicity parameter κ_{CCN}, derived from CCN measurements, is calculated from the critical supersaturation ratio (S_c) and D_{50} from the following equation [13]:

$$\kappa_{CCN} = \frac{4\mathrm{A}^3}{27D_{50}^3(lnS_c)^2}, \qquad A = \frac{4\sigma_{s/a}M_w}{RT\rho_w} \quad (2)$$

where $\sigma_{s/a}$ is the surface tension of the solution/air interface and the solution is temporarily assumed to be pure water (0.0728 N m^{-1} at 298.15 K), M_w is the molecular weight of water, R is the universal gas constant (8.314 J mol^{-1} K^{-1}), T is absolute temperature, ρ_w is the density of water.

The steepness of the AR curve represents the degree of external mixture or the heterogeneity of aerosol chemical composition, which can be quantified by the ratio of $(D_{75} - D_{25})/D_{50}$ [46]. D_{75} and D_{25} correspond to the diameters at which 75% and 25% of the particles are activated on the AR curve. Internal mixture implies that particles at any given dry size have equal κ with $(D_{75} - D_{25})/D_{50} = 0$. Alternatively, various κ at a given particle size indicate externally mixed aerosol compositions with higher $(D_{75} - D_{25})/D_c$ values. Although the sigma term from sigmoid fit has been used in previous studies to estimate aerosol mixing state [19,30], the $(D_{75} - D_{25})$ value can provide a more accurate representation of aerosol mixing state. This is because the CCN measurement uncertainties would be larger due to the extremely low concentration of activated particles at the low

AR range. In addition, the relationship between activation ratio and particle size exhibits nonlinear behavior when AR < 25% or >75% (Figure S1). In contrast, within the particle size range of D_{25} to D_{75}, the AR increases rapidly and exhibits a relatively linear relationship with the particle size. The sigma term represents the width of entire particle diameter range used in sigmoid fit. Instead of the sigma term, using the $(D_{75} - D_{25})/D_{50}$ value to describe the steepness of the AR curve can reduce the uncertainties in estimating aerosol mixing state.

2.3.2. Aerosol Hygroscopicity Derived from Aerosol Chemical Composition

The hygroscopic parameter κ is solely determined by composition and reflects the Raoult term in Köhler theory [13]. By assuming internal mixing, the aerosol hygroscopicity (κ_{chem}) can be derived from aerosol chemical composition measurements. The κ_{chem} of aerosol particles with multiple compositions is contributed by the κ of each volume-weighted composition, following the Zdanovskii–Stokes–Robinson (ZSR) mixing rule [28], expressed as:

$$\kappa_{chem} = \sum_i \varepsilon_i \kappa_i \quad (3)$$

where i represents the ith composition, ε_i is the volume fraction of each composition in the bulk, and k_i is the hygroscopic parameter for each composition present in a multiple-composition particle. For the compositions determined by ACSM the AE33 measurements, a simple ion-pairing scheme [9] was used in this study, expressed as:

$$\begin{aligned} n_{NH_4NO_3} &= n_{NO_3^-} \\ n_{H_2SO_4} &= \max\left(0, n_{SO_4^{2-}} - n_{NH_4^+} + n_{NO_3^-}\right) \\ n_{NH_4HSO_4} &= \min\left(2n_{SO_4^{2-}} - n_{NH_4^+} + n_{NO_3^-}, n_{NH_4^+} - n_{NO_3^-}\right) \\ n_{(NH_4)_2SO_4} &= \max\left(0, n_{NH_4^+} - n_{NO_3^-}\right) \\ n_{HNO_3} &= 0 \end{aligned} \quad (4)$$

All species are then converted to volume by assuming a density. The density (ρ_i) and κ_i values for all species used in this study are listed in Table 1 [15]. Here, a constant κ of 0.1 is used for particulate organics [47,48].

Table 1. Density (ρ) and hygroscopicity parameter (κ) of each pure composition used in this study.

Species	Density (kg m^{-3})	κ
NH_4NO_3	1725	0.68
$(NH_4)_2SO_4$	1769	0.52
NH_4HSO_4	1780	0.56
H_2SO_4	1830	0.92
Organics	1400	0.1
BC	1800	0

3. Results

Overview the Observation Data

The time series of meteorological parameters (such as wind speed, wind direction, ambient air temperature, and relative humidity (RH)), $PM_{2.5}$ mass concentration, N_{CN}, and N_{CCN} at SS of 0.1%, 0.2%, and 0.3% are shown in Figure 1. During the observation periods, the wind speed was mainly less than 3 m s^{-1}, with an average of 1.3 m s^{-1}. The relatively low wind speeds (<2 m s^{-1}) were generally associated with southerly winds, whereas higher wind speeds (>3 m s^{-1}) corresponded to northerly winds. When persistent southerly winds prevail (such as January 17–24th), the daily average $PM_{2.5}$ concentration and RH significantly increased from 19 to 156 μg m^{-3}, and from 31% to 77%, respectively. The cumulative enhancement of $PM_{2.5}$ concentrations was jointly influenced by local emissions, regional transport, and liquid/heterogeneous reactions at different stages of this persistent

pollution episode [49]. The RH was below 60% for most of the time, with an average of 38 ± 18%. The temperature ranged from −9 to 17 °C, with an average of 0.2 ± 4.7 °C. These meteorological parameters indicated relatively dry and cold weather conditions during this campaign.

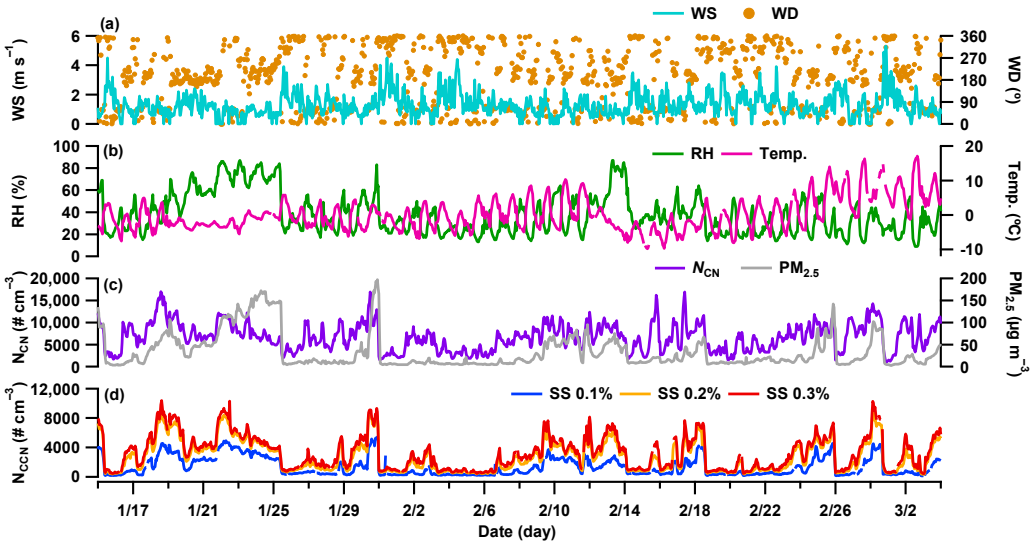

Figure 1. Time series of (**a**) wind speed (WS) and wind direction (WD); (**b**) RH and temperature; (**c**) CN number concentration (N_{CN}) and $PM_{2.5}$ mass concentration; (**d**) CCN number concentrations at SS = 0.1%, 0.2%, and 0.3% during the campaign.

The temporal variations in both aerosol number and mass concentration are shown in Figure 1c. The range of aerosol number concentration varied from ~1000 to 17,000 cm^{-3}, with an average of 6714 ± 3117 cm^{-3}. The $PM_{2.5}$ mass concentration ranged from 2 μg m^{-3} to 197 μg m^{-3}, with an average of 34 ± 39 μg m^{-3}. During the most increasing stages of $PM_{2.5}$ mass concentration, the aerosol number concentration consistently varied with the mass concentration. However, when an intermittent fog event occurred from January 23rd to 24th, the number concentration decreased with the increasing mass concentration. This suggests that the wet scavenging effect of fog droplets substantially reduced aerosol number concentration, but enhanced liquid-phase reactions alternatively resulting in the increases in mass concentration. The CCN concentration at low supersaturations (0.1%) was significantly lower than the two relatively higher supersaturations (0.2% and 0.3%) (Figure 1d), with average concentrations of 1345 ± 1270 cm^{-3}, 2752 ± 2114 cm^{-3}, and 3267 ± 2325 cm^{-3}, respectively.

The time series of $PM_{2.5}$ chemical composition, dry particle number size distribution (PNSD), and D_{50} are given in Figure 2. The particle chemical composition is closely related to its hygroscopicity and activation characteristics. The hygroscopic properties of aerosols are mainly determined by composition, with inorganics having higher hygroscopicity [9,50] than less water-soluble substances, such as BC [51,52] or primary organics [53]. At a given SS, particles with higher hygroscopicity are corresponding to smaller D_{50}, indicating such particles are more prone to activation and form cloud droplets. During the observation period, organic matter and nitrate were the most important components, with average percentages of 42.4% ± 11.9% and 21.5% ± 12.1%, respectively, followed by ammonium (18.4% ± 5.0%), sulfate (10.3% ± 7.3%), BC (5.0% ± 2.2%), and chloride (2.5% ± 1.8%), respectively. Aerosol chemical composition had a remarkable variation with $PM_{2.5}$ concentration levels, characterized by organics dominating at low $PM_{2.5}$ concentration levels (<25 μg m^{-3}) and nitrate gradually becoming the dominant composition with increases in $PM_{2.5}$ concentration. These characteristics of aerosol composition are consistent with recent studies, which reported that nitrate is now the principal component of Beijing winter haze pollution [33,34]. As a hygroscopic component, the increasing fraction of nitrate dur-

ing pollution episodes facilitates the enhancement of aerosol hygroscopicity and activity. The time series of PNSD in Figure 2b shows that aerosol particles mainly concentrate in nucleation mode (D_p < 100 nm) during the clean periods. However, as the $PM_{2.5}$ mass concentration increases, there is a significant increase in the proportion of particle numbers in the accumulation mode, accompanied by a decrease in D_{50}. The average D_{50} at SS = 0.1% (172 ± 13 nm) was significantly larger than that at SS = 0.2% (102 ± 8 nm) and SS = 0.3% (84 ± 7 nm), indicating that the SS variation was more sensitive to D_{50} at a lower SS range.

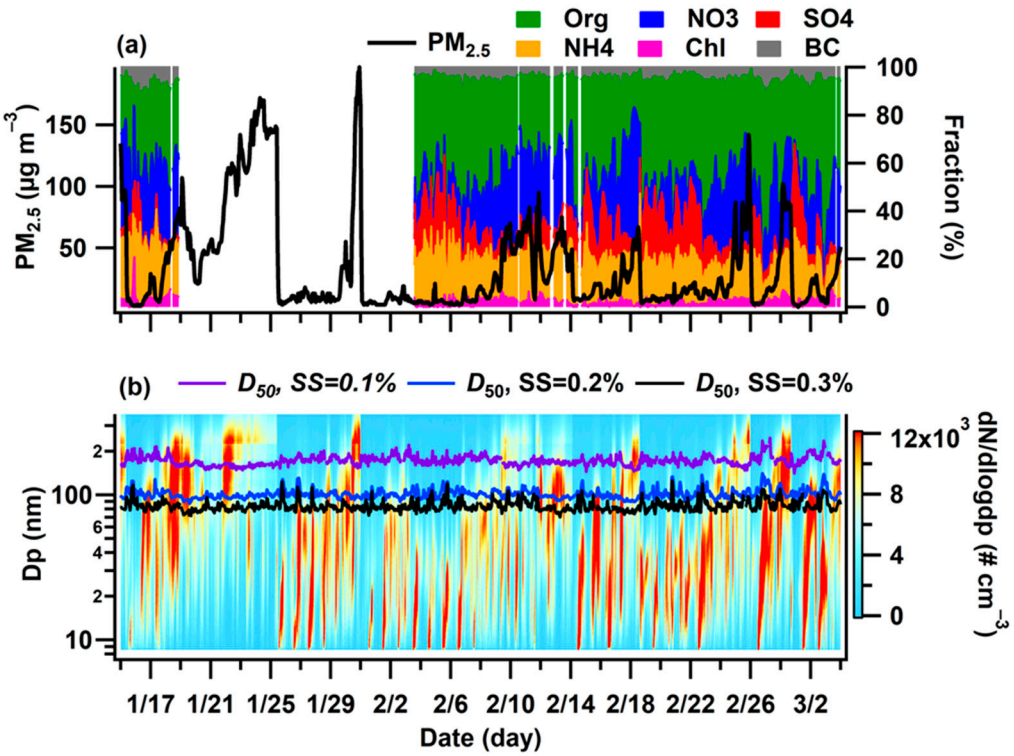

Figure 2. Temporal variations in (**a**) aerosol chemical composition along with $PM_{2.5}$ mass concentration; (**b**) particle number size distribution and critical activation diameters (D_{50}) at SS = 0.1%, 0.2%, and 0.3% during the campaign.

4. Discussion

4.1. Impacts of Aerosol Physicochemical Properties on CCN Activity

4.1.1. Aerosol Chemical Properties

The diurnal variations in D_{50} at different SS, the mass fraction of m/z 44 in organic mass spectrum (f44), aerosol chemical composition, and PNSD are given in Figure 3. The sources and properties of aerosol particles vary with different size ranges, leading to a diverse diurnal variation in D_{50} at different SS (Figure 3a–c). As a typical tracer for SOA formation, the f44 can be associated with OA hygroscopicity owing to their positive correlations reported in previous studies [54,55]. Both f44 and the sum fraction of hygroscopic inorganic components (nitrate, sulfate, and ammonium) had a noticeable peak in the afternoon (Figure 3d,e), implying they were significantly influenced by photochemical oxidation in the daytime. Meanwhile, the minimum of D_{50} for all three SS conditions occurred around 15:00, corresponding to the diurnal peak time of f44 and the fraction of inorganic components. This suggests photochemical reactions on daily basis played an important role in enhancing aerosol hygroscopicity and CCN activity.

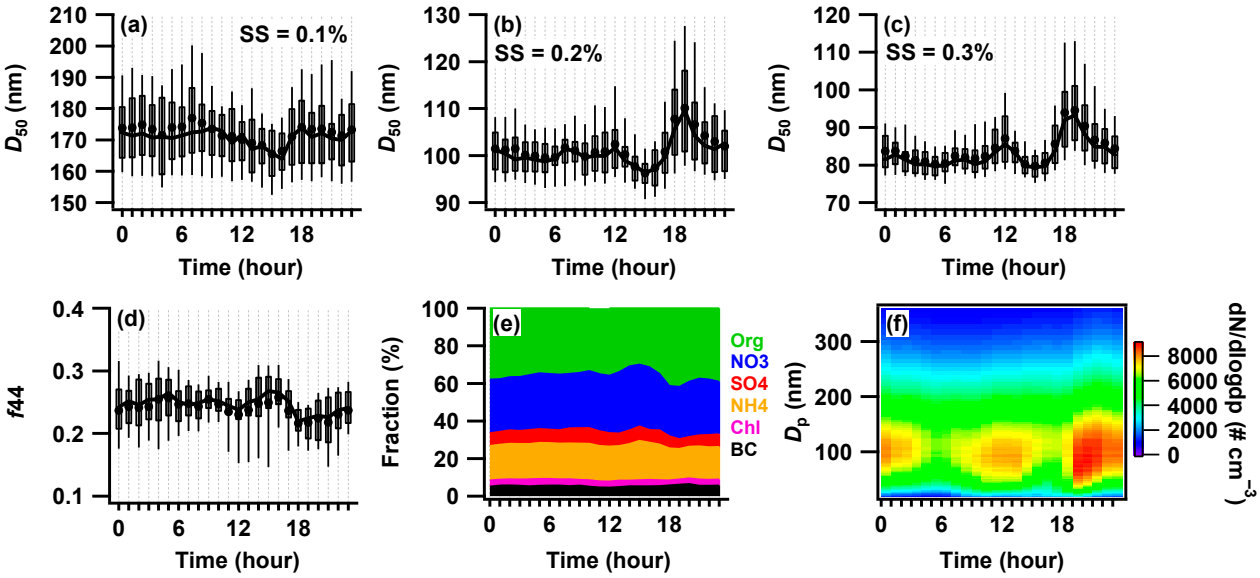

Figure 3. Diurnal variations in (**a**–**c**) critical activation diameters (D_{50}) at SS = 0.1%, 0.2%, and 0.3%, respectively; (**d**) the mass fraction of m/z 44 in organic mass spectrum ($f44$); (**e**) aerosol chemical composition; (**f**) PNSD. The lines and dots show the median and mean; box lower/higher bounds show the 25th and 75th and whiskers show the 10th and 90th percentiles.

Note that the diurnal cycles of D_{50} at SS = 0.2% and 0.3% exhibited a remarkable maximum around 18:00, with additional peaks occurring at 7:00 and 12:00. In contrast, no prominent diurnal peak occurred in the diurnal cycle of D_{50} at SS = 0.1%. Traffic and cooking emissions are the main sources of primary OA (POA) in Beijing, and these fresh emissions could lead to a decrease in $f44$ [56,57]. Therefore, the reduction time in the $f44$ diurnal cycle matched to the periods of daily source emissions, such as morning and evening traffic peaks, as well as lunch and dinner times. Consequently, the hydrophobic POA was not favor for CCN activation, leading to an increase in D_{50} at SS = 0.2% and 0.3%. In addition, the diurnal variation in aerosol number concentration within the size range of 60–150 nm was consistent with that of D_{50} (SS = 0.2% and 0.3%) (Figure 3f), indicating that particles within this size range were significantly influenced by traffic and cooking emissions. For particles larger than 150 nm, their number concentration showed no significant changes during the periods of concentrated emissions, suggesting that local primary emissions had few influences on particle properties with this size range. Therefore, there were no significant peaks observed in the diurnal variation in D_{50} at SS = 0.1%, which was generally larger than 150 nm during this campaign (Figure 3a).

The mean value of $PM_{2.5}$ mass concentration during this campaign is 25 μg m^{-3}. Once the $PM_{2.5}$ mass concentration exceeded this mean value, a period of pollution accumulation typically occurred for one to several days. Therefore, in order to further illustrate the impacts of aerosol chemical composition on CCN activity at the different pollution levels, we defined the $PM_{2.5}$ mass concentrations ≤25 μg m^{-3} and >25 μg m^{-3} as clean and polluted conditions, respectively. Note that the bulk aerosol composition measured by the ASCM is sensitive to larger particles, which contribute the majority of the total mass. Thus, the bulk composition tends to mainly reflect the composition information for larger particles. Here, only the relationships between the fraction of each chemical component and D_{50} at SS = 0.1% are presented in Figure 4. Under the polluted conditions, the fraction of nitrate increased with $PM_{2.5}$ concentrations and exhibited a negative correlation with D_{50} ($r = -0.68$), but no correlation between them ($r = 0.02$) under the clean conditions. In contrast, the fraction of sulfate only showed a correlation with D_{50} under the clean conditions ($r = -0.47$). These relationships indicated that as the concentration of $PM_{2.5}$ increases, the dominant driver of CCN activity transitioned from sulfate to nitrate. Compared with the

secondary inorganic components, both the fractions of organics and BC showed a positive correlation with D_{50} due to their limited hygroscopicity.

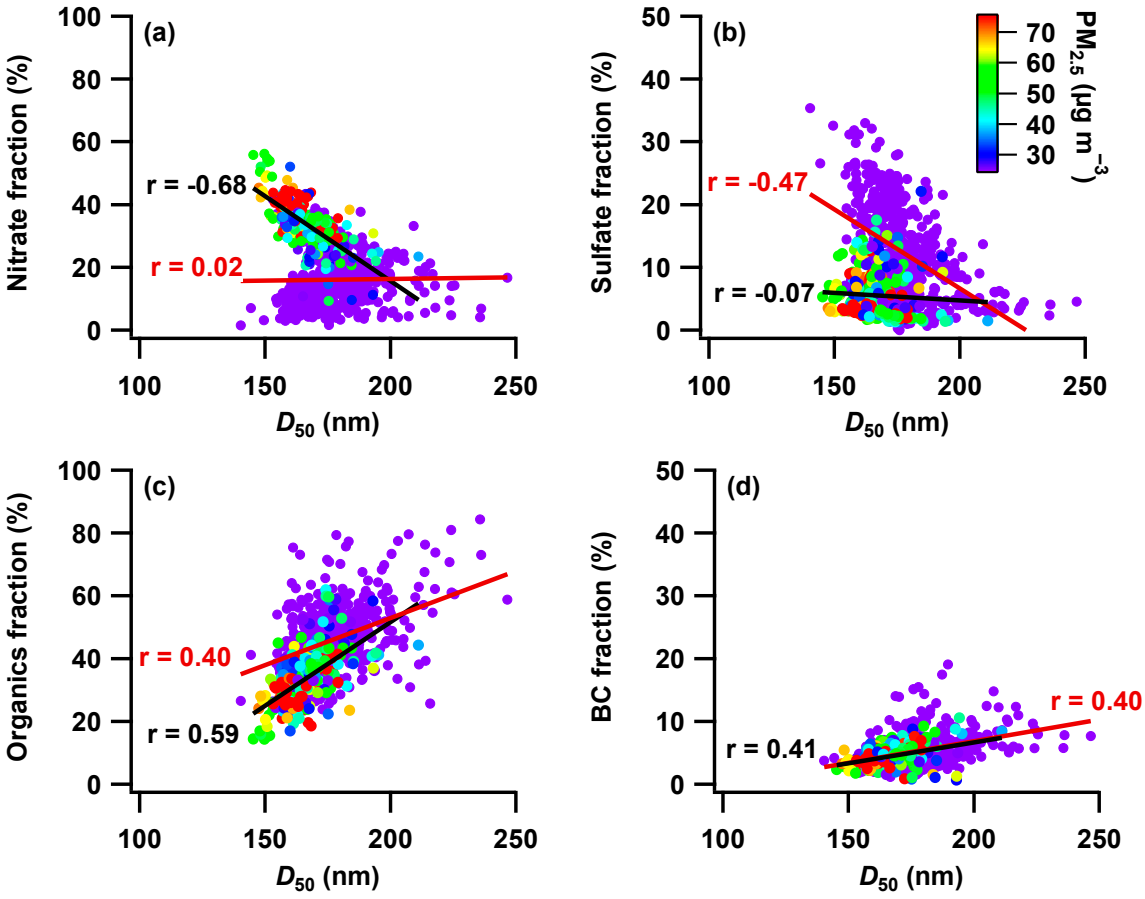

Figure 4. Correlation between the fraction of aerosol chemical components and D_{50} at SS = 0.1%. (**a**) nitrate; (**b**) sulfate; (**c**) organics; (**d**) BC. Markers are colored by the $PM_{2.5}$ mass concentration. Black and dark red lines are linear fits during the polluted periods (>25 μg m^{-3}) and clean period (≤25 μg m^{-3}), respectively.

4.1.2. Mixing State and Its Impacts on CCN Activity

As introduced in Section 2.3.1, the ratio of $(D_{75} - D_{25})/D_{50}$ can be used to describe the external-mixing degree of aerosol components. The relationships between $(D_{75} - D_{25})/D_{50}$ and D_{50} under different SS conditions are shown in Figure 5. Jurányi et al. (2013) pointed out that the $(D_{75} - D_{25})/D_{50}$ varied from 0.08 to 0.12 for ammonium sulfate calibration measurements at SS = 0.1–1.0%, which indicated an internal mixture within measurement accuracy [46]. For our measurements, the value of $(D_{75} - D_{25})/D_{50}$ distributed in a range of 0.14–0.59, with a median value of 0.31, 0.31, and 0.33 at SS = 0.1%, 0.2% and 0.3%, respectively. The higher $(D_{75} - D_{25})/D_{50}$ at SS = 0.3% suggested the smaller particles (D_p < 100 nm) tended to be more external mixing. The $(D_{75} - D_{25})/D_{50}$ in this study is significantly higher than that in a rural background site [31], where the $(D_{75} - D_{25})/D_{50}$ ranged from 0.15 to 0.20 at SS = 0.1 to 0.7%. Compared with the rural background site, aerosol particles in urban Beijing represent a more complex mixture originating from local anthropogenic emissions and regional transport.

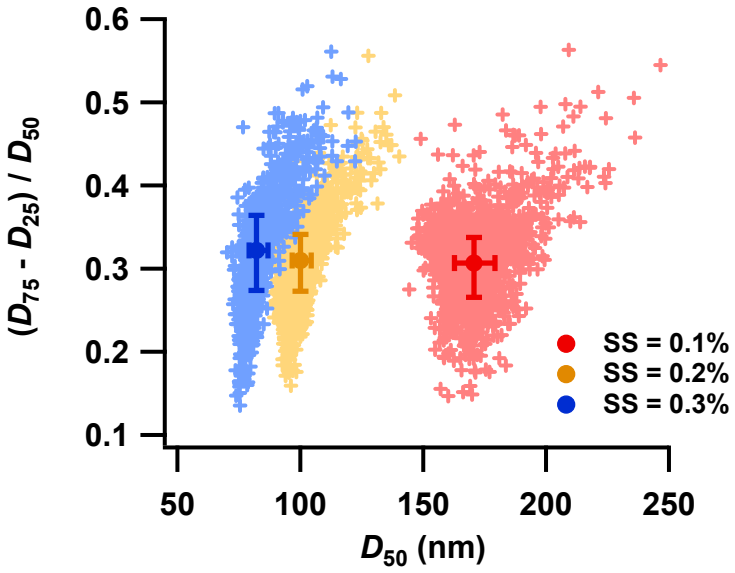

Figure 5. Correlation between the ratio of $(D_{75} - D_{25})/D_{50}$ and D_{50} at SS = 0.1%, 0.2%, and 0.3%, respectively. The solid circle, error bars denote the median, 25th and 75th percentiles, respectively.

For a specific SS, D_{50} decreased with an increase in the degree of internal mixing, implying that enhancing the internal mixing level facilitated the CCN activity. Particularly, the variation in the mixing state exhibits high sensitivity to D_{50} when the ratio drops from 0.5 to 0.3. This can be attributed to the increases in the internal mixing level during the aerosol aging process, leading to an enhancement in aerosol chemical homogeneity and hygroscopicity. The relationship between $(D_{75} - D_{25})/D_{50}$ and D_{50} can be well fitted with an exponential function under the conditions of SS = 0.2% and 0.3%. However, under the condition of SS = 0.1%, their relationship is hard to be adequately fitted. Further analysis of the relationship (SS = 0.1%) revealed that the relatively high values of $(D_{75} - D_{25})/D_{50}$ (0.3–0.4) with small D_{50} (<165 nm) occurred under high $PM_{2.5}$ concentration (>60 μg m^{-3}) and high RH (>60%) conditions (Figure S2), leading to the relationship deviated from satisfactory fitting by using an exponential function. Under these conditions, the hygroscopicity and size of aerosol particles were enlarged due to the increasing fraction of nitrate and hygroscopic growth, respectively. Especially for the fog period, the droplets had a more diverse population of κ values, as separated by some of them already condensing droplets. However, after passing through the sampling line and being dried, these enlarged particles experienced a reduction in liquid water content and particle size. As a result, the measured dry particles represent a mixture of ambient particles (or droplets) from a wider size range with various κ values, thereby exhibiting a special kind of chemical inhomogeneity.

4.2. Estimating Organic Aerosol Hygroscopicity

The size-resolved κ_{ccn} can be derived from size-resolved CCN measurements by using the D_{50} at various SS. Figure 6 shows the relationships between the κ_{ccn} and D_p at various environmental sites in China, including urban, rural, coast, and mountain sites. As can be seen, κ_{ccn} exhibited a positive correlation with D_p at most of those sites except for mountain site, which had a higher κ_{ccn} for the smaller particles. In these results, κ_{ccn} rapidly increased with particle size at the range of ~40 to 100 nm, whereas κ_{ccn} almost stays constant at D_p of 100 to 200 nm. This is consistent with previously reported results on the size-resolved aerosol chemical compositions [27], which presented a substantially varying composition within small particle size range and relatively stable compositions for larger particles. In addition, the κ_{ccn} observed at urban sites were significantly lower than that at rural sites, which can be attributed to the enhanced aerosol aging state from urban to rural

environment [14]. The κ_{chem} derived from bulk chemical composition were notably lower than κ_{ccn} during the observation periods of this study, especially for larger particle size.

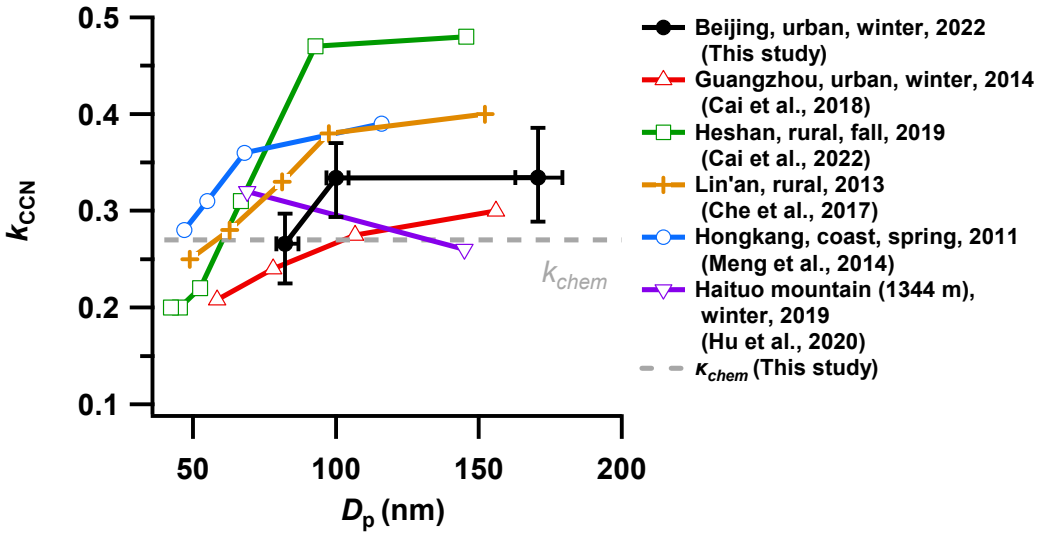

Figure 6. Size-resolved aerosol hygroscopicity parameter derived from CCN measurements at various environmental sites in China. Black solid circle and error bars denote the median, 25th and 75th percentiles, respectively, from this study. Ref. [30] for Cai et al. 2022, Ref. [29] for Cai et al. 2018, Ref. [58] for Che et al. 2017, Ref. [27] for Meng et al., 2014, Ref. [59] for Hu et al. 2020.

As the ACSM is sensitive to particle mass rather than number concentration, the bulk composition is dominated by the contribution of the larger particles. Therefore, a better correlation between κ_{chem} and κ_{ccn} was exhibited at SS of 0.1% compared with the other two SS conditions (Figures 7a and S3), suggesting the κ_{ccn} measured at SS = 0.1% was more suitable for closure analysis with κ_{chem} derived from bulk composition. Here, we assume the discrepancy between κ_{chem} and κ_{ccn} was mainly induced by the utilization of constant OA hygroscopicity parameter (κ_{org}). Then, the κ_{org} can be derived by subtracting the contribution of the inorganic salts (κ_{inorg}) from the κ_{ccn} at SS = 0.1%, expressed as:

$$\kappa_{org} = \frac{\kappa_{ccn} - \left(\kappa_{inorg}\varepsilon_{inorg} + \kappa_{BC}\varepsilon_{BC}\right)}{\varepsilon_{org}} \quad (5)$$

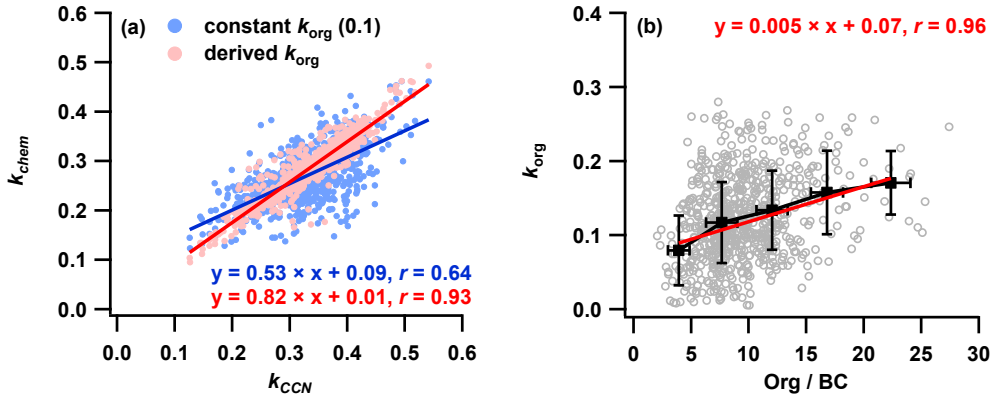

Figure 7. Relationships between (**a**) κ_{chem} and κ_{ccn}; (**b**) κ_{org} and Org/BC. Blue and grey markers in (**a**) denote κ_{chem} calculated by using constant κ_{org} of 0.1 and derived κ_{org} from Org/BC, respectively. Black squares in (**b**) denote the mean value of κ_{org} binned by Org/BC in increments of 5. Solid lines are the corresponding linear fits.

Duplissy et al. (2011) pointed out that the uncertainty in the estimation of κ_{org} decreases with increasing organic fraction; thereby, only data featuring organic fractions larger than 50% were used in this calculation [17].

As is shown in Figure 7b, the κ_{org} shows a positive relationship with the concentration ratio of organics to BC (Org/BC), which can be used to reflect the contribution of SOA to total OA [60,61]. Several previous studies suggested κ_{org} as a function of the $f44$ or O:C [54,55]; however, κ_{org} was not correlated to the $f44$ during the observation periods of this study. This is similar to a recent study conducted by Kuang et al. (2021), which pointed out that κ_{org} was weakly correlated with O:C, but well correlated with the sum mass fraction of aged biomass burning OA and more oxygenated OA in total OA [23]. In order to parameterize the relationship between κ_{org} and Org/BC ratios, κ_{org} values were binned by Org/BC in increments of 5. Then, a power fitting function $\kappa_{org} = 0.05 \times (\mathrm{Org/BC})^{0.42}$ was obtained. This fitting function was adopted to reconstruct the hygroscopicity parameter (κ_{chem_new}). As is shown in Figure 7a, a better correlation between κ_{chem} and κ_{ccn} was achieved after using the parameterized κ_{org} instead of constant value (0.1), indicating suitable κ_{org} scheme play an important role in deriving κ_{chem} from aerosol chemical composition.

5. Conclusions

The in situ measurements of CCN activity at ground level can be applied to optimize the parameters of retrieving cloud microphysics with remote sensing data. Notable reductions in $PM_{2.5}$ concentration over the past decade have been accompanied by significant changes in its chemical composition in the North China Plain. Therefore, more investigations are needed to further understand the impacts of these variations on CCN activity. In this study, aerosol size distribution, chemical composition, and CCN number concentration were measured concurrently to investigate the size-resolved CCN activity during wintertime 2022 in Beijing, China. The critical activation dimeter D_{50} derived from size-resolved activation ratio can be negatively associated with CCN activity. During the observation period, the average CCN concentrations at SS = 0.1%, 0.2%, and 0.3% were 1340 cm^{-3}, 2750 cm^{-3}, and 3270 cm^{-3}, corresponding to the average D_{50} of 172 nm, 102 nm, and 84 nm, respectively. The impacts of aerosol size distribution, chemical composition, and mixing state on CCN activity were investigated. The results show that photochemical oxidation on a daily basis played an important role in enhancing aerosol hygroscopicity and CCN activity. Conversely, the local emissions (such as traffic and cooking) significantly enhanced D_{50} at SS = 0.2% and 0.3%, but had few influences on D_{50} at SS = 0.1% due to the limitations of particle size from emission sources. As $PM_{2.5}$ concentration increases, the dominant driver of CCN activity transitions from sulfate to nitrate. For carbonaceous components, both the fractions of organics and BC showed a positive correlation with D_{50} due to their weak hygroscopicity. The mixing state of particles was also estimated based on the size-resolved AR curve fitting. At a specific SS, D_{50} decreased with increasing the degree of internal mixing, implying that the elevated internal-mixing degree resulting from atmospheric aging facilitated to the enhancement of CCN activity.

Aerosol hygroscopicity parameter κ_{ccn} derived from the SMCA method was size-dependent, varying from 0.26 to 0.34 as D_p increased from 84 to 172 nm. Based on the bulk aerosol chemical composition measured by the ACSM, the κ_{chem} values were calculated using the ZSR method. The OA hygroscopicity κ_{org} was estimated by the closure analysis between κ_{chem} and κ_{ccn}. However, the commonly used $f44$ (or O:C) was weakly correlated with κ_{org} and failed to describe the variations in κ_{org} during the observation periods of this study. Instead, the variations in κ_{org} can be well parameterized using the Org/BC ratio, which is usually used as a tracer for the contribution of SOA to total OA. The parameterization of κ_{org} substantially improved the correlation between κ_{chem} and κ_{ccn}, emphasizing the importance of considering κ_{org} variations when deriving κ_{chem} from aerosol chemical composition.

Supplementary Materials: The following supporting information can be downloaded at: https://www.mdpi.com/article/10.3390/rs15174119/s1, Figure S1: Calculation of critical activation diameter (D_{50}) for ambient aerosols; Figure S2: Correlation between the ratio of $(D_{75}-D_{25})/D_{50}$ and D_{50} at SS = 0.1%; Figure S3: Correlations between κ_{chem} and κ_{ccn} at SS of 0.2% and 0.3%, respectively.

Author Contributions: Conceptualization, Q.L. and J.S.; methodology, Q.L., X.S. and Z.L.; software, Q.L. and L.L.; validation, Q.L. and J.S.; formal analysis, J.Z. and S.L.; investigation, X.S. and L.L.; resources, H.C. and X.Z.; data curation, X.S., X.H. and W.Z.; writing—original draft preparation, Q.L. and J.S.; writing—review and editing, Y.Z. and Z.L.; supervision, X.Z.; funding acquisition, J.S. and H.C. All authors have read and agreed to the published version of the manuscript.

Funding: This study was supported in part by the National Natural Science Foundation of China (Nos. 42030608, 42090031, 42275121, 41975177, 42175128), in part by the Chinese Academy of Meteorological Sciences (Nos. 2023Z012, 2022KJ002, 2022KJ005). It was also supported by the Innovation Team for Haze-fog Observation and Forecasts of Ministry of Science and Technology of China.

Data Availability Statement: The data presented in this study are available on request from the corresponding author.

Conflicts of Interest: The authors declare no conflict of interest.

References

1. Köhler, H. The nucleus in and the growth of hygroscopic droplets. *Trans. Faraday Soc.* **1936**, *32*, 1152–1161. [CrossRef]
2. Dusek, U.; Frank, G.; Hildebrandt, L.; Curtius, J.; Schneider, J.; Walter, S.; Chand, D.; Drewnick, F.; Hings, S.; Jung, D.; et al. Size matters more than chemistry for cloud-nucleating ability of aerosol particles. *Science* **2006**, *312*, 1375–1378. [CrossRef] [PubMed]
3. Charlson, R.J.; Schwartz, S.E.; Hales, J.M.; Cess, R.D.; Coakley, J.A., Jr.; Hansen, J.E.; Hofmann, D.J. Climate forcing by anthropogenic aerosols. *Science* **1992**, *255*, 423–430. [CrossRef] [PubMed]
4. Twomey, S. The nuclei of natural cloud formation part II: The supersaturation in natural clouds and the variation of cloud droplet concentration. *Pure Appl. Geophys.* **1959**, *43*, 243–249. [CrossRef]
5. IPCC. *Climate Change 2021: The Physical Science Basis, Contribution of Working Group I to the Sixth Assessment Report of the Intergovernmental Panel on Climate Change*; Cambridge University Press: Cambridge, UK, 2021; p. 959. [CrossRef]
6. Kacarab, M.; Thornhill, K.L.; Dobracki, A.; Howell, S.G.; O'Brien, J.R.; Freitag, S.; Poellot, M.R.; Wood, R.; Zuidema, P.; Redemann, J.; et al. Biomass burning aerosol as a modulator of the droplet number in the southeast Atlantic region. *Atmos. Chem. Phys.* **2020**, *20*, 3029–3040. [CrossRef]
7. Andreae, M.; Rosenfeld, D. Aerosol-cloud-precipitation interactions. Part 1. The nature and sources of cloud-active aerosols. *Earth-Sci. Rev.* **2008**, *89*, 13–41. [CrossRef]
8. Farmer, D.K.; Cappa, C.D.; Kreidenweis, S.M. Atmospheric Processes and Their Controlling Influence on Cloud Condensation Nuclei Activity. *Chem. Rev.* **2015**, *115*, 4199. [CrossRef]
9. Gysel, M.; Crosier, J.; Topping, D.O.; Whitehead, J.D.; Bower, K.N.; Cubison, M.J.; Williams, P.I.; Flynn, M.J.; McFiggans, G.B.; Coe, H. Closure study between chemical composition and hygroscopic growth of aerosol particles during TORCH2. *Atmos. Chem. Phys.* **2007**, *7*, 6131–6144. [CrossRef]
10. Feingold, G. Modeling of the first indirect effect: Analysis of measurement requirements. *Geophys. Res. Lett.* **2003**, *30*, 1–4. [CrossRef]
11. Ervens, B.; Feingold, G.; Kreidenweis, S.M. Influence of water-soluble organic carbon on cloud drop number concentration. *J. Geophys. Res. Atmos.* **2005**, *110*, D18211. [CrossRef]
12. Zhang, Q.; Meng, J.; Quan, J.; Gao, Y.; Zhao, D.; Chen, P.; He, H. Impact of aerosol composition on cloud condensation nuclei activity. *Atmos. Chem. Phys.* **2012**, *12*, 3783–3790. [CrossRef]
13. Petters, M.D.; Kreidenweis, S.M. A single parameter representation of hygroscopic growth and cloud condensation nucleus activity. *Atmos. Chem. Phys.* **2007**, *7*, 1961–1971. [CrossRef]
14. Zhang, Q.; Jimenez, J.L.; Canagaratna, M.R.; Allan, J.D.; Coe, H.; Ulbrich, I.; Alfarra, M.R.; Takami, A.; Middlebrook, A.M.; Sun, Y.L.; et al. Ubiquity and dominance of oxygenated species in organic aerosols in anthropogenically-influenced Northern Hemisphere midlatitudes. *Geophys. Res. Lett.* **2007**, *34*, L13801. [CrossRef]
15. Liu, Q.; Liu, D.; Gao, Q.; Tian, P.; Wang, F.; Zhao, D.; Bi, K.; Wu, Y.; Ding, S.; Hu, K.; et al. Vertical characteristics of aerosol hygroscopicity and impacts on optical properties over the North China Plain during winter. *Atmos. Chem. Phys.* **2020**, *20*, 3931–3944. [CrossRef]
16. Wang, Y.H.; Liu, Z.R.; Zhang, J.K.; Hu, B.; Ji, D.S.; Yu, Y.C.; Wang, Y.S. Aerosol physicochemical properties and implications for visibility during an intense haze episode during winter in Beijing. *Atmos. Chem. Phys.* **2015**, *15*, 3205–3215. [CrossRef]
17. Duplissy, J.; DeCarlo, P.F.; Dommen, J.; Alfarra, M.R.; Metzger, A.; Barmpadimos, I.; Prevot, A.S.H.; Weingartner, E.; Tritscher, T.; Gysel, M.; et al. Relating hygroscopicity and composition of organic aerosol particulate matter. *Atmos. Chem. Phys.* **2011**, *11*, 1155–1165. [CrossRef]

18. Mei, F.; Setyan, A.; Zhang, Q.; Wang, J. CCN activity of organic aerosols observed downwind of urban emissions during CARES. *Atmos. Chem. Phys.* **2013**, *13*, 12155–12169. [CrossRef]
19. Mei, F.; Wang, J.; Zhou, S.; Zhang, Q.; Collier, S.; Xu, J. Measurement report: Cloud condensation nuclei activity and its variation with organic oxidation level and volatility observed during an aerosol life cycle intensive operational period (ALC-IOP). *Atmos. Chem. Phys.* **2021**, *21*, 13019–13029. [CrossRef]
20. Wu, Z.J.; Zheng, J.; Shang, D.J.; Du, Z.F.; Wu, Y.S.; Zeng, L.M.; Wiedensohler, A.; Hu, M. Particle hygroscopicity and its link to chemical composition in the urban atmosphere of Beijing, China, during summertime. *Atmos. Chem. Phys.* **2016**, *16*, 1123–1138. [CrossRef]
21. Chang, R.Y.W.; Slowik, J.G.; Shantz, N.C.; Vlasenko, A.; Liggio, J.; Sjostedt, S.J.; Leaitch, W.R.; Abbatt, J.P.D. The hygroscopicity parameter (κ) of ambient organic aerosol at a field site subject to biogenic and anthropogenic influences: Relationship to degree of aerosol oxidation. *Atmos. Chem. Phys.* **2010**, *10*, 5047–5064. [CrossRef]
22. Rickards, A.M.J.; Miles, R.E.H.; Davies, J.F.; Marshall, F.H.; Reid, J.P. Measurements of the Sensitivity of Aerosol Hygroscopicity and the κ Parameter to the O/C Ratio. *J. Phys. Chem. A* **2013**, *117*, 14120–14131. [CrossRef] [PubMed]
23. Kuang, Y.; Huang, S.; Xue, B.; Luo, B.; Song, Q.; Chen, W.; Hu, W.; Li, W.; Zhao, P.; Cai, M.; et al. Contrasting effects of secondary organic aerosol formations on organic aerosol hygroscopicity. *Atmos. Chem. Phys.* **2021**, *21*, 10375–10391. [CrossRef]
24. Moore, R.H.; Bahreini, R.; Brock, C.A.; Froyd, K.D.; Cozic, J.; Holloway, J.S.; Middlebrook, A.M.; Murphy, D.M.; Nenes, A. Hygroscopicity and composition of Alaskan Arctic CCN during April 2008. *Atmos. Chem. Phys.* **2011**, *11*, 11807–11825. [CrossRef]
25. Deng, Z.; Zhao, C.; Ma, N.; Liu, P.; Ran, L.; Xu, W.; Chen, J.; Liang, Z.; Liang, S.; Huang, M.; et al. Size-resolved and bulk activation properties of aerosols in the North China Plain. *Atmos. Chem. Phys.* **2011**, *11*, 3835–3846. [CrossRef]
26. Moore, R.H.; Cerully, K.; Bahreini, R.; Brock, C.A.; Middlebrook, A.M.; Nenes, A. Hygroscopicity and composition of California CCN during summer 2010. *J. Geophys. Res. Atmos.* **2012**, *117*, D00V12. [CrossRef]
27. Meng, J.W.; Yeung, M.C.; Li, Y.J.; Lee, B.Y.L.; Chan, C.K. Size-resolved cloud condensation nuclei (CCN) activity and closure analysis at the HKUST Supersite in Hong Kong. *Atmos. Chem. Phys.* **2014**, *14*, 10267–10282. [CrossRef]
28. Stokes, R.H.; Robinson, R.A. Interactions in Aqueous Nonelectrolyte Solutions. I. Solute-Solvent Equilibria. *J. Phys. Chem.* **1966**, *70*, 2126–2131. [CrossRef]
29. Cai, M.; Huang, S.; Liang, B.; Sun, Q.; Liu, L.; Yuan, B.; Shao, M.; Hu, W.; Chen, W.; Song, Q.; et al. Measurement report: Distinct size dependence and diurnal variation in organic aerosol hygroscopicity, volatility, and cloud condensation nuclei activity at a rural site in the Pearl River Delta (PRD) region, China. *Atmos. Chem. Phys.* **2022**, *22*, 8117–8136. [CrossRef]
30. Cai, M.; Tan, H.; Chan, C.K.; Qin, Y.; Xu, H.; Li, F.; Schurman, M.I.; Liu, L.; Zhao, J. The size-resolved cloud condensation nuclei (CCN) activity and its prediction based on aerosol hygroscopicity and composition in the Pearl Delta River (PRD) region during wintertime 2014. *Atmos. Chem. Phys.* **2018**, *18*, 16419–16437. [CrossRef]
31. Wang, Y.; Henning, S.; Poulain, L.; Lu, C.; Stratmann, F.; Wang, Y.; Niu, S.; Pöhlker, M.L.; Herrmann, H.; Wiedensohler, A. Aerosol activation characteristics and prediction at the central European ACTRIS research station of Melpitz, Germany. *Atmos. Chem. Phys.* **2022**, *22*, 15943–15962. [CrossRef]
32. Action Plan on Prevention and Control of Air Pollution (Chinese State Council, 2013). Available online: http://www.gov.cn/zwgk/2013-09/12/content_2486773.htm (accessed on 19 January 2022). (In Chinese)
33. Zhai, S.; Jacob, D.J.; Wang, X.; Liu, Z.; Wen, T.; Shah, V.; Li, K.; Moch, J.M.; Bates, K.H.; Song, S.; et al. Control of particulate nitrate air pollution in China. *Nat. Geosci.* **2021**, *14*, 389–395. [CrossRef]
34. Zhang, Y.; Tian, J.; Wang, Q.; Qi, L.; Manousakas, M.I.; Han, Y.; Ran, W.; Sun, Y.; Liu, H.; Zhang, R.; et al. High-time-resolution chemical composition and source apportionment of PM2.5 in northern Chinese cities: Implications for policy. *EGUsphere* **2023**, *2023*, 1–33. [CrossRef]
35. Li, H.; Cheng, J.; Zhang, Q.; Zheng, B.; Zhang, Y.; Zheng, G.; He, K. Rapid transition in winter aerosol composition in Beijing from 2014 to 2017: Response to clean air actions. *Atmos. Chem. Phys.* **2019**, *19*, 11485–11499. [CrossRef]
36. Tuch, T.M.; Haudek, A.; Müller, T.; Nowak, A.; Wex, H.; Wiedensohler, A. Design and performance of an automatic regenerating adsorption aerosol dryer for continuous operation at monitoring sites. *Atmos. Meas. Tech.* **2009**, *2*, 417–422. [CrossRef]
37. Hu, X.; Sun, J.; Xia, C.; Shen, X.; Zhang, Y.; Liu, Q.; Liu, Z.; Zhang, S.; Wang, J.; Yu, A.; et al. Measurement report: Rapid decline of aerosol absorption coefficient and aerosol optical property effects on radiative forcing in an urban area of Beijing from 2018 to 2021. *Atmos. Chem. Phys.* **2023**, *23*, 5517–5531. [CrossRef]
38. Xia, C.; Sun, J.; Hu, X.; Shen, X.; Zhang, Y.; Zhang, S.; Wang, J.; Liu, Q.; Lu, J.; Liu, S.; et al. Effects of hygroscopicity on aerosol optical properties and direct radiative forcing in Beijing: Based on two-year observations. *Sci. Total Environ.* **2023**, *857*, 159233. [CrossRef] [PubMed]
39. Moore, R.H.; Nenes, A.; Medina, J. Scanning Mobility CCN Analysis—A Method for Fast Measurements of Size-Resolved CCN Distributions and Activation Kinetics. *Aerosol Sci. Technol.* **2010**, *44*, 861–871. [CrossRef]
40. Middlebrook, A.M.; Bahreini, R.; Jimenez, J.L.; Canagaratna, M.R. Evaluation of Composition-Dependent Collection Efficiencies for the Aerodyne Aerosol Mass Spectrometer using Field Data. *Aerosol Sci. Technol.* **2012**, *46*, 258–271. [CrossRef]
41. Canagaratna, M.R.; Jayne, J.T.; Jimenez, J.L.; Allan, J.D.; Alfarra, M.R.; Zhang, Q.; Onasch, T.B.; Drewnick, F.; Coe, H.; Middlebrook, A.; et al. Chemical and microphysical characterization of ambient aerosols with the aerodyne aerosol mass spectrometer. *Mass Spectrom. Rev.* **2007**, *26*, 185–222. [CrossRef]

42. Fröhlich, R.; Cubison, M.J.; Slowik, J.G.; Bukowiecki, N.; Prévôt, A.S.H.; Baltensperger, U.; Schneider, J.; Kimmel, J.R.; Gonin, M.; Rohner, U.; et al. The ToF-ACSM: A portable aerosol chemical speciation monitor with TOFMS detection. *Atmos. Meas. Tech.* **2013**, *6*, 3225–3241. [CrossRef]
43. Drinovec, L.; Močnik, G.; Zotter, P.; Prévôt, A.S.H.; Ruckstuhl, C.; Coz, E.; Rupakheti, M.; Sciare, J.; Müller, T.; Wiedensohler, A.; et al. The "dual-spot" Aethalometer: An improved measurement of aerosol black carbon with real-time loading compensation. *Atmos. Meas. Tech.* **2015**, *8*, 1965–1979. [CrossRef]
44. Hagen, D.E.; Alofs, D.J. Linear Inversion Method to Obtain Aerosol Size Distributions from Measurements with a Differential Mobility Analyzer. *Aerosol Sci. Technol.* **1983**, *2*, 465–475. [CrossRef]
45. Deng, Z.Z.; Zhao, C.S.; Ma, N.; Ran, L.; Zhou, G.Q.; Lu, D.R.; Zhou, X.J. An examination of parameterizations for the CCN number concentration based on in situ measurements of aerosol activation properties in the North China Plain. *Atmos. Chem. Phys.* **2013**, *13*, 6227–6237. [CrossRef]
46. Jurányi, Z.; Tritscher, T.; Gysel, M.; Laborde, M.; Gomes, L.; Roberts, G.; Baltensperger, U.; Weingartner, E. Hygroscopic mixing state of urban aerosol derived from size-resolved cloud condensation nuclei measurements during the MEGAPOLI campaign in Paris. *Atmos. Chem. Phys.* **2013**, *13*, 6431–6446. [CrossRef]
47. Dusek, U.; Frank, G.P.; Curtius, J.; Drewnick, F.; Schneider, J.; Kürten, A.; Rose, D.; Andreae, M.O.; Borrmann, S.; Pöschl, U. Enhanced organic mass fraction and decreased hygroscopicity of cloud condensation nuclei (CCN) during new particle formation events. *Geophys. Res. Lett.* **2010**, *37*, L03804. [CrossRef]
48. Gunthe, S.S.; Rose, D.; Su, H.; Garland, R.M.; Achtert, P.; Nowak, A.; Wiedensohler, A.; Kuwata, M.; Takegawa, N.; Kondo, Y.; et al. Cloud condensation nuclei (CCN) from fresh and aged air pollution in the megacity region of Beijing. *Atmos. Chem. Phys.* **2011**, *11*, 11023–11039. [CrossRef]
49. Zhong, J.; Zhang, X.; Dong, Y.; Wang, Y.; Wang, J.; Zhang, Y.; Che, H. Feedback effects of boundary-layer meteorological factors on explosive growth of $PM_{2.5}$ during winter heavy pollution episodes in Beijing from 2013 to 2016. *Atmos. Chem. Phys.* **2018**, *18*, 247–258. [CrossRef]
50. Cruz, C.; Pandis, S. Deliquescence and Hygroscopic Growth of Mixed Inorganic−Organic Atmospheric Aerosol. *Environ. Sci. Technol.* **2000**, *34*, 4313–4319. [CrossRef]
51. Aklilu, Y.; Mozurkewich, M.; Prenni, A.J.; Kreidenweis, S.M.; Alfarra, M.R.; Allan, J.D.; Anlauf, K.; Brook, J.; Leaitch, W.R.; Sharma, S. Hygroscopicity of particles at two rural, urban influenced sites during Pacific 2001: Comparison with estimates of water uptake from particle composition. *Atmos. Environ.* **2006**, *40*, 2650–2661. [CrossRef]
52. Pringle, K.J.; Tost, H.; Pozzer, A.; Pöschl, U.; Lelieveld, J. Global Distribution of the Effective Aerosol Hygroscopicity Parameter for CCN Activation. *Atmos. Chem. Phys.* **2010**, *10*, 5241–5255. [CrossRef]
53. Wang, J.; Lee, Y.-N.; Daum, P.H.; Jayne, J.; Alexander, M.L. Effects of aerosol organics on cloud condensation nucleus (CCN) concentration and first indirect aerosol effect. *Atmos. Chem. Phys.* **2008**, *8*, 6325–6339. [CrossRef]
54. Wu, Z.J.; Poulain, L.; Henning, S.; Dieckmann, K.; Birmili, W.; Merkel, M.; van Pinxteren, D.; Spindler, G.; Müller, K.; Stratmann, F.; et al. Relating particle hygroscopicity and CCN activity to chemical composition during the HCCT-2010 field campaign. *Atmos. Chem. Phys.* **2013**, *13*, 7983–7996. [CrossRef]
55. Kuang, Y.; He, Y.; Xu, W.; Zhao, P.; Cheng, Y.; Zhao, G.; Tao, J.; Ma, N.; Su, H.; Zhang, Y.; et al. Distinct diurnal variation in organic aerosol hygroscopicity and its relationship with oxygenated organic aerosol. *Atmos. Chem. Phys.* **2020**, *20*, 865–880. [CrossRef]
56. Liu, Q.; Sun, Y.; Hu, B.; Liu, Z.R.; Akio, S.; Wang, Y.S. In situ measurement of PM1 organic aerosol in Beijing winter using a high-resolution aerosol mass spectrometer. *Chin. Sci. Bull.* **2012**, *57*, 819–826. [CrossRef]
57. Sun, Y.L.; Wang, Z.F.; Fu, P.Q.; Yang, T.; Jiang, Q.; Dong, H.B.; Li, J.; Jia, J.J. Aerosol composition, sources and processes during wintertime in Beijing, China. *Atmos. Chem. Phys.* **2013**, *13*, 4577–4592. [CrossRef]
58. Che, H.C.; Zhang, X.Y.; Zhang, L.; Wang, Y.Q.; Zhang, Y.M.; Shen, X.J.; Ma, Q.L.; Sun, J.Y.; Zhong, J.T. Prediction of size-resolved number concentration of cloud condensation nuclei and long-term measurements of their activation characteristics. *Sci. Rep.* **2017**, *7*, 5819. [CrossRef]
59. Hu, D.; Liu, D.; Zhao, D.; Yu, C.; Liu, Q.; Tian, P.; Bi, K.; Ding, S.; Hu, K.; Wang, F.; et al. Closure Investigation on Cloud Condensation Nuclei Ability of Processed Anthropogenic Aerosols. *J. Geophys. Res.-Atmos.* **2020**, *125*, e2020JD032680. [CrossRef]
60. Aiken, A.C.; Salcedo, D.; Cubison, M.J.; Huffman, J.A.; DeCarlo, P.F.; Ulbrich, I.M.; Docherty, K.S.; Sueper, D.; Kimmel, J.R.; Worsnop, D.R.; et al. Mexico City aerosol analysis during MILAGRO using high resolution aerosol mass spectrometry at the urban supersite (T0)—Part 1: Fine particle composition and organic source apportionment. *Atmos. Chem. Phys.* **2009**, *9*, 6633–6653. [CrossRef]
61. Liu, Q.; Sheng, J.; Wu, Y.; Ma, Z.; Sun, J.; Tian, P.; Zhao, D.; Li, X.; Hu, K.; Li, S.; et al. Source characterization of volatile organic compounds in urban Beijing and its links to secondary organic aerosol formation. *Sci. Total Environ.* **2023**, *860*, 160469. [CrossRef]